Applied Catalysis B: Environmental 339 (2023) 123114

Contents lists available at ScienceDirect

Applied Catalysis B: Environmental

journal homepage: www.elsevier.com/locate/apcatb

An ultra-long stability of lanthanum (La) modified molecular sieve for catalytic degradation of typical sulfur-containing VOCs in a near-real environment

Jichang Lu [a,c,e,1], Rui Tian [a,c,e,1], Wenjun Zhang [a,c,e], Yilin Zhang [a], Yijia Yang [a], Zhizhi Xu [b,c,d,e], Dedong He [b,c,e], Tianhao Ai [a,b,c,e,*], Yongming Luo [a,b,c,e,*]

[a] Faculty of Environmental Science and Engineering, Kunming University of Science and Technology, Kunming 650500, PR China
[b] Faculty of Chemical Engineering, Kunming University of Science and Technology, Kunming 650500, PR China
[c] The Innovation Team for Volatile Organic Compounds Pollutants Control and Resource Utilization of Yunnan Province, Kunming 650500, PR China
[d] Yunnan Research Academy of Eco-environmental Sciences, Kunming 650034, PR China
[e] The Higher Educational Key Laboratory for Odorous Volatile Organic Compounds Pollutants Control of Yunnan Province, Kunming 650500, PR China

ARTICLE INFO

Keywords:
Mixed sulfur-containing VOCs
Ethyl mercaptan
Deactivation mechanism
Moisture resistance

ABSTRACT

The catalytic degradation of typical sulfur-containing VOCs, ethyl mercaptan (C_2H_5SH), in a near-real environment remains a challenge task. In this study, an ultra-long stability of 600 h for degradation of C_2H_5SH was obtained over La doped ZSM-5, and the corresponding catalytic performance, reaction and deactivation mechanism were investigated by a series of ex situ and in situ characterizations. Furthermore, the influence law of other low-carbon mercaptans, such as methyl mercaptan (CH_3SH), propyl mercaptan (C_3H_7SH), and butyl mercaptan (C_4H_9SH) as well as the moisture on their stability were investigated. The slight deactivation by designed experiment revealed a distinguished reversible moisture-induced deactivation mechanism, where moisture promoted the formation of carbonate related species that covers the active sites, while this deactivation could be recovered by a simple temperature-lifting strategy. This work provides a theoretical guidance for catalytic degradation of mixed sulfur-containing VOCs under the presence of moisture.

1. Introduction

Volatile organic compounds (VOCs) produced by the industrial exploitation as well as the energy transformation and utilization have photochemical reaction properties when they were emitted into atmospheric environment, which can lead to severe environmental pollution problems. For instance, VOCs not only would react photochemically with nitrogen oxides (NO_x) under ultraviolet rays to produce harmful photochemical oxidants such as O_3, but also can be converted into secondary organic aerosols to participate in the formation of secondary particulate matter inducing haze. Meanwhile, most of VOCs have uncomfortable odor and/or physiological toxicity, which will cause serious harm to human health [1]. Low-carbon mercaptans (R-SH, R= C_nH_{2n+2}, n = 1, 2, 3 and 4) are a type of sulfur-containing VOCs with particularly awful odor, high toxicity, and severe corrosion, which are widely generated from the transformation and utilization of hydrocarbon fuels, such as coals, natural gases and petroleum fuels [2]. Among them, ethyl mercaptan (C_2H_5SH) has the minimum odor threshold value of 0.7 μg/L and is considered as the smelliest gas in the word claimed by the Guinness Book of World Records. Therefore, the effective removal of high-toxic low-carbon sulfur-containing VOCs, particular C_2H_5SH, is of great importance to improve the atmospheric environment and human health.

Various methods are available to remove C_2H_5SH, which include absorption and adsorption [3–5], catalytic decomposition (combustion) [6–9], photo-catalysis [10–12], biodegradation [13], etc. Compared with other technologies, the catalytic decomposition technique does not require the addition of any reagents and can be converted into the valuable basic materials of hydrogen sulfide and ethene, becoming one of the most promising routes for removing the medium and high concentration of C_2H_5SH [14]. Zeolite-like materials are the most promising and widely investigated catalysts for the catalytic decomposition of

* Corresponding authors at: Faculty of Environmental Science and Engineering, Kunming University of Science and Technology, Kunming 650500, PR China.
E-mail addresses: aith@kust.edu.cn (T. Ai), environcatalysis@kust.edu.cn (Y. Luo).
[1] These authors contributed equally to this work.

https://doi.org/10.1016/j.apcatb.2023.123114
Received 11 April 2023; Received in revised form 30 June 2023; Accepted 17 July 2023
Available online 18 July 2023

C_2H_5SH due to the low cost, high efficiency and environmental benign as well as their acid-catalyzed properties. Especially, the acidic properties can guarantee the complete transformation of C_2H_5SH into hydrogen sulfide and ethene. Previous research works mainly focused on improving the catalytic activity and investigating the reaction mechanism for the degradation of C_2H_5SH over various kinds of zeolite and its modified materials, such as typical X, Y and ZSM-5 zeolite. For example, metal cations (cadmium and mercury) doped NaX were reported to obtain a 100% desulfurization efficiency of C_2H_5SH at 450 °C, and the catalytic activity of C_2H_5SH was found to have a well relationship with the ion-exchange degree [15]. Ziolek and coworkers reported that C_2H_5SH molecules could be effectively chemisorbed on the acid and basic centers of alkali metals doped NaY zeolites via coordination and/or hydrogen bonds, which promotes the cleavage of C-S bond [7]. Recently, Hulea and coworkers [6,16] demonstrated that C_2H_5SH could be directionally converted to H_2S over ZSM-5 with respect to other zeolites, and the complete conversion of C_2H_5SH could be arrived at 400 °C and the selectivity of H_2S was as high as 93%. Nevertheless, all the reported literature are not paid attention to the catalytic stability as well as the corresponding deactivation mechanism for decomposing C_2H_5SH. More importantly, the catalytic decomposition of C_2H_5SH in a real environment (including the coexisting sulfur-containing VOCs and the widely present moisture) still remains a challenge.

In many actual environments such as coal gasification, various kinds of sulfur-containing VOCs are generally co-presented in an environment of high-moisture and high-temperature. At present, the catalytic degradation of mixed oxygen/nitrogen-containing VOCs has emerged as a hot research subject. In general, there are some differences in the catalytic activity and stability between the decomposition of single and multiple VOCs, and the decomposition behaviors of multi-component VOCs are often more complex than those of one component [17,18]. Hence, it is difficult to predict the decomposition behaviors of mixed-component VOCs only based on the well-known catalytic behaviors of one component VOCs [19,20]. According to the previous documents, the effects of co-existing VOCs on catalytic performances can be generally classified into mutual inhibition, mutual independence and synergistic promotion [21,22]. The mutual inhibition role was the commonly presented behaviors during the catalytic decomposition of VOCs. Ortiz et al. investigated and compared the catalytic oxidation of chlorinated VOCs (dichloromethane, trichloroethylene, n-hexane, and their mixtures) over CeO_2, ZrO_2, and $Ce_xZr_{1-x}O_2$ catalysts, a remarkable mutual inhibition effects was found for oxidation decomposition of mixed VOCs due to the competition of VOCs over the same active sites [21]. In contrast, a synergistic promotion effect was found during the catalytic oxidation of a mixture of acetone, ethyl acetate, and toluene, where the addition of acetone and ethyl acetate decrease the T_{50} value for the conversion of toluene from 214 to 158 °C via changing the rate-determining step of ring-opening process [22]. However, the catalytic behaviors for decomposing ethyl mercaptan with the presence of other sulfur-containing VOCs (mainly CH_3SH, C_3H_7SH, and C_4H_9SH) has rarely been reported, hindering the researches progress to design long stability catalysts and the practical application of designed catalysts [6,23].

The performance of catalytic decomposition of VOCs in a near-real environment is not only related to the similar sulfur-containing components but also influenced by the presence of moisture. The effect of moisture on the catalytic combustion of VOCs is very complex and shows different effects in different catalytic oxidation processes, including the direct reaction with the active noble metals to deactivate the catalyst; inhibiting the reduction of metal oxide catalysts, and the competing with reactants over adsorption sites to reduce the catalytic activity [24–26]. In the catalytic combustion of toluene, the increase in the concentration of water vapor from 0% to 10% decreased the toluene conversion by about 23% over $CuO/\gamma\text{-}Al_2O_3$ [27]. Nevertheless, in catalytic oxidation of benzene, the addition of moisture improved the conversion of benzene from 20% to 40% over $MnO_x/\gamma\text{-}Al_2O_3$ catalyst [28]. The result suggests that the intermediate by-products may be reacted rapidly in the presence of moisture to avoid competing with benzene over the catalytic active site, thus improving the catalytic activity. Thus, in general, moisture plays a complex role in the catalytic combustion of VOCs, while the influence of moisture on the reaction and deactivation mechanism for the catalytic degradation of sulfur-containing VOCs, especially C_2H_5SH, is rarely reported and needs to be deeply investigated.

In our previous studies, a lot of works has focused on the catalytic decomposition of one component of methyl mercaptan (CH_3SH) over ZSM-5 and its modified catalysts [29–31]. Among them, the modification of acidic HZSM-5 with an alkaline lanthanum (La) largely decreased the formation of deposited coke and sulfur, and obtained the longest lifetime for decomposing CH_3SH (~80 h) as well as the excellent regeneration ability (no deactivation signs after five cycles) [32]. However, the catalytic decomposition of sulfur-containing VOCs in a real environment (especially, the coexisting sulfur components and the widely present moisture) is still lacking [23]. Investigating the catalytic decomposition of ethyl mercaptan with the presence of other mercaptan mixtures as well as the moisture can build a bridge between theoretical research and practical application and further guide the actual pollution control of sulfur-containing VOCs.

In this work, ZSM-5-based catalysts doped with La and yttrium (Y) as a typical representative of light and heavy rare earths respectively were selected for the catalytic decomposition of C_2H_5SH. A comprehensive knowledge of the physicochemical properties of La and Y modified catalysts, and the corresponding reaction and deactivation mechanism for the decomposition of C_2H_5SH were investigated by characterizations of N_2 adsorption and desorption, X-ray diffraction (XRD), temperature programmed desorption of CO_2/NH_3/RSH (CO_2/NH_3/RSH-TPD), X-ray photoelectron spectroscopy (XPS) and in-situ diffuse reflectance infrared Fourier transform spectroscopy (in situ DRIFTS), etc. Moreover, the influence of other mercaptans (CH_3SH, C_3H_7SH and C_4H_9SH) as well as the presence of moisture on the catalytic decomposition of C_2H_5SH over La-Z catalyst in a near-real environment were deeply discussed. This work greatly expands our understanding of the influence law of catalytic decomposition of sulfur-containing VOCs with hazardous and malodorous nature in a near-real environment.

2. Experimental section

2.1. Catalyst preparation

All the chemicals and reagents were used without further purification. Lanthanum(III) nitrate hexahydrate ($La(NO_3)_3{\cdot}6\ H_2O$) as well as Yttrium(III) nitrate hexahydrate ($Y(NO_3)_3{\cdot}6\ H_2O$) were purchased from Shanghai Chemical Reagent Co., Ltd. The molecular sieve of ZSM-5 was bought from Fuzhou Zeolite Co., Ltd. ZSM-5 was first pretreated by calcination in a muffle furnace at 550 °C for 5 h. The 13 wt% of rare earth (La and Y) modified ZSM-5 catalysts were prepared by wetting chemical impregnation method [32,33]. Typically, a certain content of rare earth precursors was diluted with DI water. With stirring, two grams of ZSM-5 carrier was slowly added to the above solutions to ensure a complete wetting of the support. The final mixture was stand for 12 h, and then dried at 120 °C for 6 h. The dried samples were ground and calcined at 550 °C for 5 h in a muffle furnace. Fresh ZSM-5, La and Y modified ZSM-5 were labeled as Z5-F, La-Z5-F and Y-Z5-F, respectively.

2.2. Catalyst characterizations

Several techniques were employed to characterize catalyst samples. Surface area and pore volume were measured by using a micron-sized ASAP 2020 instrument and all the samples were degassed at 250 °C under vacuum for 4 h prior to the measurement. Powder X-ray diffraction (XRD) was performed on a Rigaku D/Max-1200 diffractometer (Rigaku, Tokyo, Japan) with Cu Kαradiation (λ= 0.15406 nm),

operating at 40 kV and 30 mA. The data of samples were recorded at 2θ range of 5–90° with the scanning rate of 2–4°/min. X-ray photoelectron spectroscopy (XPS) was conducted on a PHI 5000 Versa Probe II with non-monochromatic Al Ka radiation (1486.6 eV) as the excitation X-ray source to determine the chemical state and surface element composition of all the samples. Si $2p_{3/2}$ at 103.3 eV and C1s at 284.8 eV were used to account for charging effects, and a Casa XPS processing program was employed for background subtraction and peak fitting. FT-IR spectra of the samples in the form of KBr pellets with a spectral resolution of 4 cm^{-1} at room temperature were recorded by using a Nicolet 560 infrared spectrometer. Thermogravimetric (TG) analysis was performed by using a thermogravimetric analyzer Q500 in which the used samples were heated from room temperature to 800 °C under air with a heating rate of 20 °C/min. A high resolution Al solid state nuclear magnetic resonance (NMR) experiment was conducted on Bruker AVANCE III 600 spectrometer equipped with a 4 mm triple resonance probe operating at a resonance frequency of 156.4 MHz. Transmission electron microscopy (TEM) image was obtained on a JEM-2100Plus electron microscope. The surface morphology of the samples was characterized using a TESCAN MIRA LMS scanning electronic microscopy (SEM). The elemental mappings of Si, Al, La, Y were obtained by an energy dispersive spectroscopy with a model of QuorumSC7620.

NH_3-TPD and CO_2-TPD were employed to determine the acid-base characteristics of the obtained samples, in which an online thermal conductivity detector (TCD) was applied to record the desorbed ammonia and carbon dioxide, respectively. In a typical measurement batch, 100 mg of catalyst sample was pretreated under 450 °C for 0.5 h and cooled down to 100 °C in the flow of high-purity helium (30 mL/min, WHSV about 9 000 $mL{\cdot}g^{-1}h^{-1}$). Then, 10 vol% of NH_3 or CO_2 (balanced with He, 30 mL/min) was introduced into the reactor for 2 h to saturate the acid or alkaline sites of the measured samples, respectively. Subsequently, the saturated sample was treated with the flow of high-purity helium (30 mL/min) under 100 °C for 1 h to remove the weak and/or physical adsorbed ammonia or carbon dioxide. Finally, the temperature was increased from 30 °C to 700 °C with the heating rate of 10 °C/min, and the desorption of NH_3 or CO_2 was measured by one online gas chromatographs (GC) equipped with a highly sensitive thermal conductivity detector (TCD).

Mercaptan-temperature programmed desorption (abbreviated as RSH-TPD) was used to further investigate the desorption performances together with reaction mechanism for the decomposing CH_3SH or C_2H_5SH over La-Z5-F. Before measurement, La-Z5-F was pretreated under 550 °C for 1 h and then cooled to 50 °C in the flow of air. After that, the pretreated sample was adsorbed and saturated with CH_3SH or C_2H_5SH (5000 ppm, balanced with N_2) under 50 °C for 12 h, followed by the treatment with the flow of high-purity N_2 at 50 °C to eliminate the physical adsorption of CH_3SH or C_2H_5SH. Finally, RSH-TPD measurement was performed at temperature region between 50 °C and 500 °C with the heating rate of 1 °C/min in the flow of high-purity N^2. The corresponding products were analyzed by using two online gas chromatographs (GCs) equipped with a thermal conductivity detector (TCD), a flame photometric detector (FPD), two flame ionization detectors (FIDs) and a methanation reactor.

In-situ diffuse reflectance infrared Fourier transform spectroscopy (DRIFTS) was recorded using an IS50 FT-IR spectrometer equipped with ZnSe windows and a high-temperature heating chamber. Prior to the measurement, the sample was charged into the IR cell and treated at 450 °C for 0.5 h and cooled down to 50 °C in the flow of N_2 (30 mL/min). After the background spectrum was recorded, the mixed gases of C_2H_5SH/N_2 (0.5%/99.5%) was introduced to the measurement system. At the same time, the temperature was increased from 50° to 450°C with the heating rate of 10 °C/min, and the corresponding spectra of in situ DRIFTS to detect the adsorbed species on the surface of catalyst were collected.

2.3. Catalytic activity and stability tests

The catalytic activity of C_2H_5SH decomposition was carried out in a fixed-bed quartz reactor with the continuous flow at atmospheric pressure. Typically, 200 mg of catalyst sample with the particle size between 0.25 and 0.38 nm was loaded into the reactor, and the feed mixture gas containing 5000 ppm of C_2H_5SH (balanced with N_2) with a gas flow rate of 30 mL/min was introduced into the reaction system so as to maintain weight-hourly space velocity (WHSV) of 9000 $mL{\cdot}g^{-1}h^{-1}$. In order to evaluate the effects of co-existed low-carbon mercaptans on the catalytic stability of C_2H_5SH, other experimental conditions are well consistent with those of the activity experiment except that the feed mixture gases (C_2H_5SH and N_2) were replaced and the test temperature was fixed at 450 °C. Herein, the feed mixture gases containing both C_2H_5SH and low-carbon mercaptans (CH_3SH, C_3H_7SH and C_4H_9SH) were introduced into the reaction system, and the corresponding compositions within the feed gases were $CH_3SH/C_2H_5SH/N_2$ (2500 ppm CH_3SH and 2500 ppm C_2H_5SH, balanced with N_2), $C_3H_7SH/C_2H_5SH/N_2$ (2500 ppm C_3H_7SH and 2500 ppm C_2H_5SH, balanced with N_2), $C_4H_9SH/C_2H_5SH/N_2$ (2500 ppm C_4H_9SH and 2500 ppm C_2H_5SH, balanced with N_2). Furthermore, in order to investigate the influence of moisture on the catalytic stability of La-Z5-F, the feed mixture gases containing of C_2H_5SH, CH_3SH and H_2O were introduced into the reaction system to keep the WHSV of 15000 $mL{\cdot}g^{-1}h^{-1}$, and the corresponding compositions within the feed gases are $CH_3SH/C_2H_5SH/H_2O/N_2$ (250 ppm CH_3SH and 250 ppm C_2H_5SH, 10 vol% H_2O, balanced with N_2). As for kinetic measurements, the conversion of C_2H_5SH was kept below 20% to ensure that the reaction is within the kinetic regime. Then, the apparent activation energy was calculated based on the Arrhenius equation. The reactants and reaction products were detected by using two online gas chromatographs (GCs) equipped with one TCD, one FPD, two FID detectors together with one methanation reactor, and the corresponding conversion of low-carbon mercaptans was calculated according to the following equation:

$$\text{MercaptansConversion}(\%) = \frac{c_{in}-c_{out}}{c_{in}} \times 100\%$$

where C_{in} represents the inlet concentration of low-carbon mercaptans before the reaction and C_{out} is the out concentration of them after the reaction.

2.4. Thermodynamic calculation

Whether a chemical reaction can occur or not requires both thermodynamic and kinetic conditions to be satisfied, in which the thermodynamic parameters will describe the likelihood of the reaction occurring and the kinetic parameters will elaborate the rate of the reaction occurs. In general, the thermodynamic data (the changes of Gibbs free energy and enthalpy, equilibrium constant) of many reactions can be directedly obtained from HSC Chemistry software. However, due to the lack of the fundamental parameter about low-carbon mercaptans in the software, therefore, the corresponding thermodynamics data of C_2H_5SH can only calculate in light of Kirchhoff's law, Gibbs-Helmholtz's law, and their modified equations [34,35]. On the basis of thermodynamic data, assuming that the reaction rate of C_2H_5SH is based on a quasi-primary reaction, kinetic equations have been developed to estimate the values of kinetic parameters for the decomposition of C_2H_5SH over La-Z5-F and to calculate the apparent activation energy based on the Arrhenius equation.

3. Results and discussion

3.1. Identification of the catalytic activity difference for C_2H_5SH decomposition

The catalytic activities for the decomposition of C_2H_5SH over Z5-F, La-Z5-F and Y-Z5-F were compared and shown in Fig. 1A. As seen, the

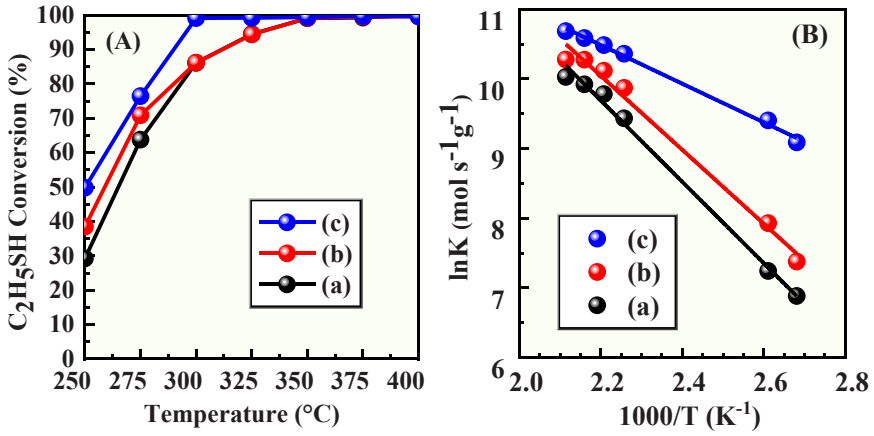

Fig. 1. (A) Temperature dependence of C_2H_5SH conversion and (B) Kinetic diagrams of catalysts (a = Z5-F, b = Y-Z5-F and c = La-Z5-F).

complete conversion of C_2H_5SH over Z5-F can be achieved at 350 °C, while the addition of Y into ZSM-5 does not change the temperature of 100% conversion but slightly promotes the catalytic performance in the low temperature region. Compared to Z5-F, La-Z5-F shows significant improvements both in the low-temperature conversion and the corresponding temperature of complete conversion (from 350 °C to 300 °C), indicating the promotion effect in the catalytic activity for decomposing C_2H_5SH. Apparent activation energy is a very effective and convincing tool to evaluate the promotion role of catalyst. Based on kinetic experiments and the Arrhenius equation, as shown in Fig. 1B and Table 1, the corresponding apparent activation energy of La-Z5-F (23.07 kJ/mol) is far lower than that of Y-Z5-F (44.12 kJ/mol) and Z5-F (48.53 kJ/mol), which are well consistent with the results obtained for catalytic activity test. Thus, all the obtained results provide a direct and credible evidence to prove the promotion effect of La species on decomposing C_2H_5SH.

N_2 adsorption-desorption isotherms of Z5-F, La-Z5-F and Y-Z5-F are displayed in Fig. 2A, and the corresponding physicochemical properties are summarized in Table 1. According to the IUPAC classification, the isotherms of the three samples are type I, implying the presence of the typical microporous structures [36]. With the addition of La and Y into ZSM-5, the specific surface area, pore volume and micropore pore volume decrease to some degree, which might be closely associated with the fact that some La or Y species have entered the original channel of parent ZSM-5. The XRD patterns of Z5-F, La-Z5-F and Y-Z5-F are shown in Fig. 2B. Compared to Z5-F, the diffraction peaks indexed to mordenite framework inverted (MFI) structure are still observed in the patterns of La-Z5-F and Y-Z5-F, indicating that the original zeolitic characteristics is well maintained [37]. Meanwhile, it is also noted the intensities of all diffraction peaks over La-Z5-F and Y-Z5-F with respect to Z5-F decrease to a great degree, which may be due to the presence of some La or Y oxides inside the ZSM-5 channel. A slight shift of the characteristic peaks of Y-Z5-F and La-Z5-F compared to Z5-F is also observed in inset of Fig. 2, suggesting the replacement of a smaller radius of Al^{3+} by a larger radius of La^{3+} that causes a lattice expansion. A high resolution solid-state Al NMR in Fig. S1 shows a slight shift of main peak at 57 ppm characteristic of the tetra-coordinated Al in ZSM-5 framework, illustrating the possible local environment change of Al species, which also proves the replacement of a portion of the skeletal aluminum (Al) via the addition of La species [30,38]. Furthermore, the diffraction peaks assigned to La and Y oxides are not detected in the patterns of La-Z5-F and Y-Z5-F, owing to the formation of the small grains of La/Y species or the highly dispersed La/Y species generated from the replacement of Al species [39]. TEM and HRTEM images of La-Z5-F and Y-Z5-F in Fig. S2 confirm that no distinct La and Y nanoparticles are observed. SEM images and the corresponding mapping of Y-Z5-F and La-Z5-F in Fig. S3 prove the presence of a highly and uniform dispersed La and Y species. NH_3-TPD and CO_2-TPD are used to determine the acid-base properties to disclose the cause of the difference in catalytic activity. NH_3-TPD and CO_2-TPD profiles of Z5-F, La-Z5-F and Y-Z5-F are illustrated in Fig. 2C and 2D, respectively, and the corresponding amount of acid and base sites are tabulated in Table 1. As displayed in Fig. 2C, two peaks located at 240 °C and 440 °C are observed for Z5-F, La-Z5-F and Y-Z5-F, which are attributed to weak acid sites and strong acid sites originating from extra-framework Al and framework Al, respectively [40]. Notably, the amount of both the weak acid sites and strong acid sites of La-Z5-F (439.5 and 294.5 μmol/g) and Y-Z5-F (551.2 and 305.1 μmol/g) are far lower than those of Z5-F (756.5 and 568.8 μmol/g). In the reported literature, a higher amount of acid sites was believed to correspond to a higher catalytic activity, while this result is contrary to the catalytic activity order in Fig. 1. One of reason is probably due to a higher amount of acid sites resulting in the deposition of more sulfur and carbon species, which would cover the active sites and hamper the catalytic activity [16]. Moreover, it is possible that enough acid sites are present over La-Z5-F to satisfy the sites-requirement for decomposing C_2H_5SH. In fact, the decrease in the strength and amount of both the weak acid and strong acid sites over La-Z5-F can reduce the deposition of carbon and/or sulfur species, which are responsible for the improvement in the catalytic stability [16]. Another interesting phenomenon is observed in the change of basic sites for three samples. It is found that the basic sites of La-Z5-F (37.6 μmol/g) and Y-Z5-F (29.8 μmol/g) are higher than those of Z5-F (22.3 μmol/g), which are in the following order: La-Z5-F > Y-Z5-F > Z5-F. The increasing in the number of basic sites would be closely associated with the improvement of catalytic activity particularly at the low-temperature region, which is due to the promotional role of more basic sites on the adsorption and activation of acidic C_2H_5SH molecules.

Table 1
Physicochemical properties and apparent activation energies of Z5-F, La-Z5-F and Y-Z5-F.

Catalysts	S_{BET} (m^2/g)	V_p (cm^3/g)	Acidity (μmolg^{-1})[a]		Basicity (μmolg^{-1})	E_a (kJ/mol)[b]
			Weak	Strong		
La-Z5-F	170.7	0.08	439.5	294.5	37.6	23.07
Y-Z5-F	135.8	0.05	551.2	305.1	29.8	44.12
Z5-F	317.0	0.14	756.5	568.8	22.3	48.53

S_{BET}: BET surface area was calculated by using Brumauer-Emmett-Teller (BET) mode.
V_p: single point adsorption total pore volume.
[a] Determined by quantifying the desorption peak area from NH_3/CO_2-TPD profiles.
[b] Apparent activation energy.

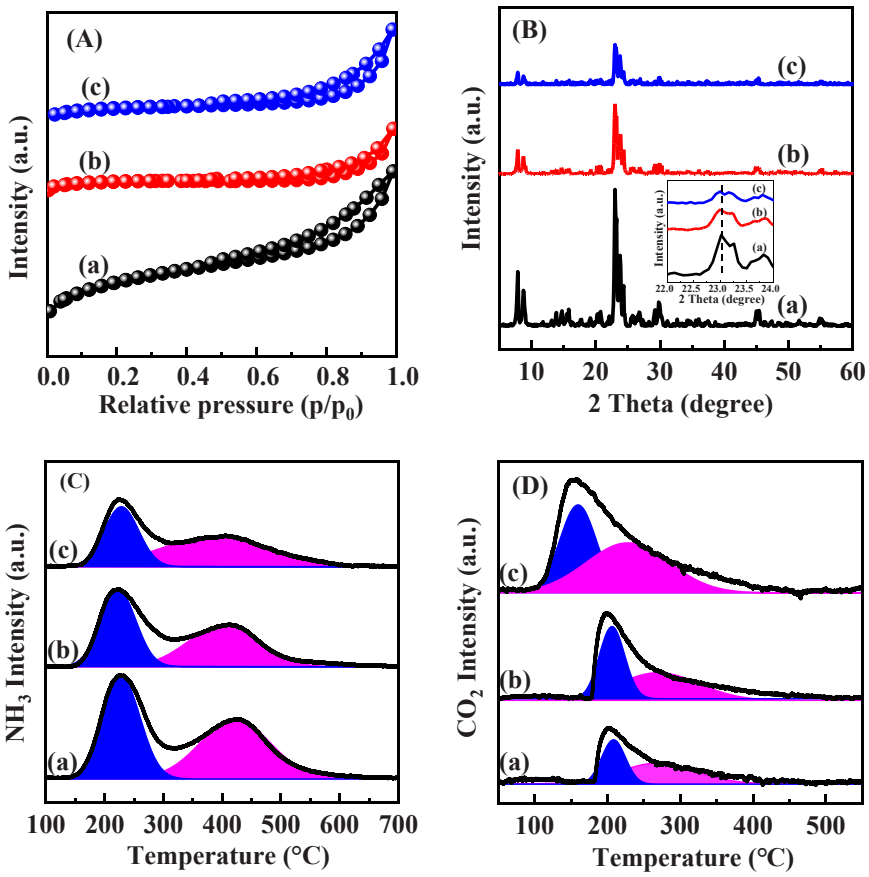

Fig. 2. (A) N_2 adsorption-desorption isotherms, (B) XRD patterns, (C) NH_3-TPD, and (D) CO_2-TPD profiles of catalysts (a: Z5-F, b: Y-Z5-F and c: La-Z5-F).

3.2. Unraveling the role of La on improving stability for decomposing C_2H_5SH

In addition to the promotion role in catalytic activity, the addition of La species also largely improves the stability, as shown in Fig. 3. It is seen that the lifetime of ZSM-5 for decomposing C_2H_5SH can maintain 230 h and then the conversion gradually decreases from 100% to 40%. However, La-Z catalyst shows no deactivation sign during time on stream of 600 h, proving that the addition of La significantly improves the catalytic stability for the decomposition of C_2H_5SH. The promoted effect and the deactivation causes were further analyzed by XPS. XPS spectra of Z5-F and La-Z5-F as well as the corresponding samples after reaction of 230 h and 600 h, named as Z-R230 and La-Z-R600, respectively, were used to determine the nature of La, sulfur and carbon related species. It is seen in Fig. 4A that the binding energy of 835.34 eV is present over La-Z5-F, proving the presence of La_2O_3 related species [32]. As known, the binding energy of 164.1 eV is attributed to elemental sulfur (S^0), and the signal at 168.0 eV is assigned to sulfate species (SO_4^{2-}) [32,41]. As seen in Fig. 5B, it is found that large amounts of elemental sulfur as well as sulfate species are detected in the deactivated ZSM-5 catalyst, while only a small fraction of sulfate species and no elemental sulfur are observed for La-Z-R600 after reaction of 600 h. Those results indicate that the production of elemental sulfur species is one of main cause for catalyst deactivation, which has a certain difference with traditional metal oxides that sulfate was the main cause for deactivation. C 1 s XPS spectra is used to infer whether the deposited coke is presented. Both Z-R230 and La-Z-R600 in Fig. 4C show three convolution peaks. The peak at 284.8 eV is attributed to the presence of C═C bonded compounds, the binding energies at 286.3 and 289.2 eV are ascribed to C-O bond, and carbonate species, respectively. Distinctly, the deactivated ZSM-5 catalyst has a higher amount of polyolefins and carbonate species, indicating that the deposition of these carbon species

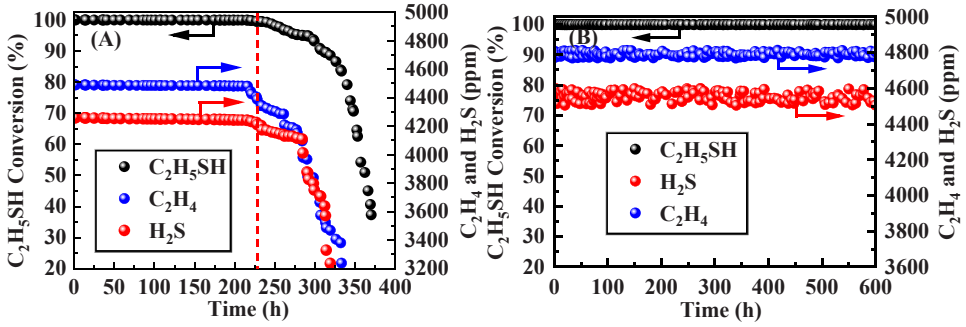

Fig. 3. The stability tests for the decomposition of C_2H_5SH, including the conversion and the dominant reaction products (C_2H_4 and H_2S) over (A) Z5-F and (B) La-Z5-F.

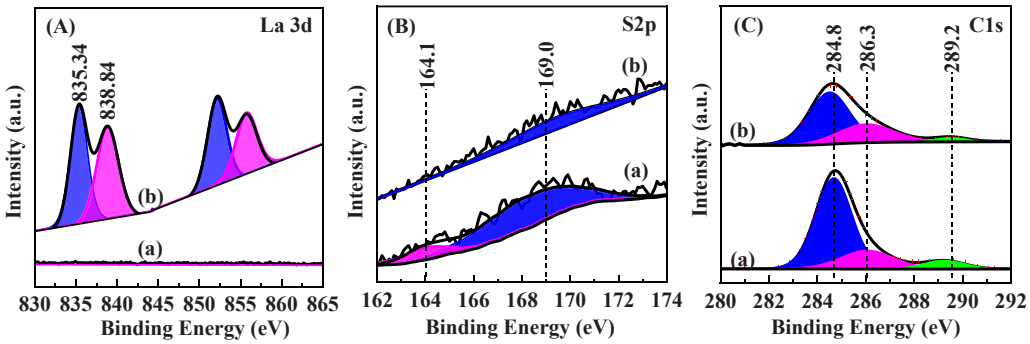

Fig. 4. (A) La 3d XPS spectra of (a) Z5-F and (b) La-Z5-F. (B) S2p and (C) C1s XPS spectra of Z5-F and La-Z5-F catalysts after stability test for decomposing C_2H_5SH (a: Z5-R-230, b: La-Z5-R-600).

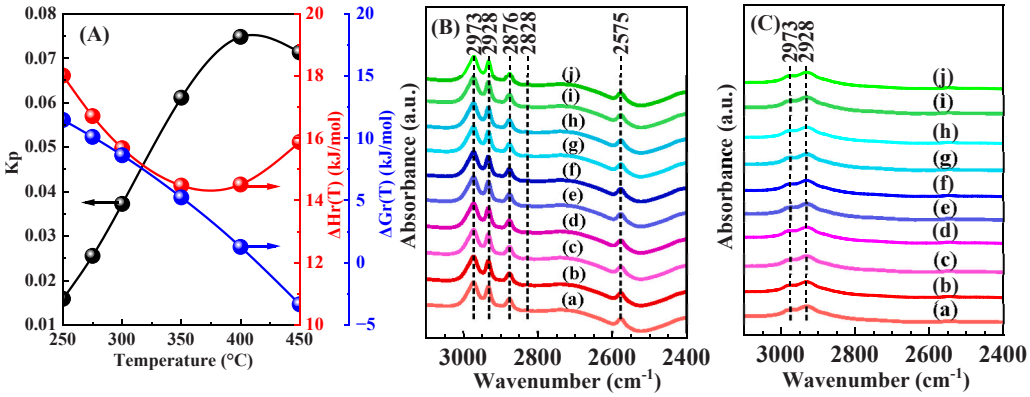

Fig. 5. Thermodynamic data of the decomposition of C_2H_5SH (A). *In situ* DRIFTS spectra of C_2H_5SH decomposition over La-Z5-F at different reaction times (a=3 s, b=5 s, c=10 s, d=15 s, e=30 s, f=40 s, g=50 s, h=60 s, i = 90 s, j = 120 s, the infrared instrument scan time was not included) at the temperature of 100 °C (B) and 400 °C (C).

is also one of the catalyst deactivation causes. In all, the deactivation of parent ZSM-5 is due to the covering of the active sites by both complex deposited carbon and elemental sulfur species. The enhanced stability of La doped ZSM-5 is related to the decrease in the acidity as well as the increase in the alkalinity that inhibited the deposition of coke and elemental sulfur, and prevented catalyst deactivation [32].

3.3. *Revealing the reaction mechanism for decomposing C_2H_5SH*

The stability experiment mentioned above demonstrates that only the products of ethene (C_2H_4) and H_2S were detected, indicating that the decomposition of C_2H_5SH follows the equation of $C_2H_5SH = C_2H_4 + H_2S$ with a theoretic stoichiometric ratio of 1:1:1. A subtle difference between theoretic and practical stoichiometric ratios among C_2H_5SH, C_2H_4 and H_2S in Fig. 3 is possibly due to either the strong adsorption of polar molecules by the spatial confinement effect of ZSM-5 or the deposition of some solid sulfur and carbon species over the catalyst surface [42,43]. The thermodynamic calculations were used to verify the feasibility for the catalytic decomposition of C_2H_5SH. As seen in Fig. 5 A, the reaction for the decomposition of C_2H_5SH displays the positive values of ΔHr (T) and ΔGr (T) as well as a small value of K_p (<1), indicating that this is an endothermic reaction and can not occur spontaneously in thermodynamics. It is believed that from the viewpoint of thermodynamics that the decomposition of C_2H_5SH into ethylene and hydrogen sulfide is not favorable, while the reaction performance largely depends on the activity of catalysts.

To further verify the key intermediates, reaction pathways, and reaction mechanisms for the decomposition of C_2H_5SH, in situ DRIFTS experiment of La-Z5-F was carried out, as shown in Figs. 5B and 5C. Several typical infrared regions in the range of 2800–3200 cm^{-1} and 2500–2600 cm^{-1} are observed. Usually, the bands around 2960–2970 cm^{-1} and 2870–2880 cm^{-1} are assigned to asymmetric and symmetric C-H stretching vibrations of methylene (CH_3) groups, i.e. $\upsilon_{as}(CH_3)$ and $\upsilon_s(CH_3)$, while 2920–2930 cm^{-1} and 2840–2850 cm^{-1} are associated with asymmetric and symmetric C-H stretching vibrations, namely $\upsilon_{as}(CH_2)$ and $\upsilon_s(CH_2)$, respectively [32,44,45]. Moreover, the peaks at 2560–2580 cm^{-1} are usually assigned to S-H stretching vibration (υ_{SH}) [46–48]. Based on these determined assignment analyses, the adsorption behavior and reaction mechanism for decomposing C_2H_5SH are further revealed. As can be seen in Fig. 5B, when the temperature is 100 °C, the infrared signals exhibit four characteristic peaks at 2973 and 2876 cm^{-1} as well as 2928 and 2828 cm^{-1}, typically attributed to the groups of $*CH_3$ and $*CH_2$ in the molecule of C_2H_5SH, respectively. Meanwhile, the band at 2575 cm^{-1} assigned to the fragment of *SH also appears. These results indicate that the C-S bond in C_2H_5SH starts to break even at low temperature, promoting the generation of the groups of $*CH_3CH_2$ and *SH. Notably, as the reaction time progresses, both the signals of $*CH_3CH_2$ and *SH remain stable, suggesting that the dissociation of C_2H_5SH molecule occurs at the millisecond level. With the temperature arrives at 400 °C (Fig. 5C), the intensities of all the peaks attributed to $*CH_3CH_2$ species weaken, revealing that those species as a key reaction intermediates are further converted. Meanwhile, the species of *SH at 2575 cm^{-1} disappears, and the intensity of $*CH_3$ species at 2973 cm^{-1} becomes weaker than that of $*CH_2$ species. These observations suggest that the reaction mechanism at high temperature follows the occurrence of dissociation of CH_3CH_2* into adsorbed CH_2CH_2* and *H as well as the rearrangement of *SH with *H to generate the gaseous of H_2S. The microscopic elementary reaction steps for the catalytic decomposition of C_2H_5SH is provided as followed.

C_2H_5SH (g) → C_2H_5SH*

C_2H_5SH* → C_2H_5* + *SH

C_2H_5* → C_2H_4* + *H

*SH + *H → *H_2S

*H_2S → H_2S (g)

C_2H_4* → C_2H_4 (g)

3.4. Investigation the influence of co-existed low-carbon mercaptans

Considering that S-VOCs with carbon and sulfur elements could easily deactivate the catalysts, this is a big improvement in the stability of La-Z5-F catalyst for the catalytic decomposition of typical sulfur-containing VOCs. The excellent stability indicates that La/Z5-F has potential commercial value and application prospects for the catalytic decomposition of C_2H_5SH. However, it is noted that the above study mainly focused on the treatment of single component of S-VOCs. In practice, the generation of C_2H_5SH is usually accompanied with other sulfur-containing VOCs, such as CH_3SH, C_3H_7SH, and C_4H_9SH. Therefore, the effect of the addition of other sulfur-containing VOCs on the stability of C_2H_5SH over La/Z5 should be further investigated. The stability tests for decomposition of two components mercaptans, i.e., C_2H_5SH vs CH_3SH, C_2H_5SH vs C_3H_7SH, C_2H_5SH vs C_4H_9SH over La-Z5-F catalyst were carried out, as shown in Figs. 6(A), 6(B) and 6(C), respectively. When CH_3SH was added to C_2H_5SH (Fig. 6A), it can be seen that the stability of C_2H_5SH dropped dramatically from 600 h over single component system to 65 h over mixed system, indicating that the addition of CH_3SH has a very serious effect on the stability of C_2H_5SH. However, the addition of C_3H_7SH and C_4H_9SH do not affect the stability for the decomposition of two components mixed mercaptans (Figs. 6B, and 6C). These results show that there may be the presence of a complex effect of CH_3SH on decomposing C_2H_5SH in the mixing reaction process compared to other mercaptans.

Competitive adsorption is a common phenomenon that multiple gas components compete with each other over adsorption sites when the catalysis reaction takes place on the catalyst surface. Depending on whether the adsorption sites are unique or not, the competing adsorption processes can be simply classified into two types: the different gas components have independent adsorption sites as well as the different gas components have the same type of adsorption sites [49–51]. The competitive adsorption of a mixtures of mercaptans over La-Z5-F can also affect the interaction between the mercaptan molecules and active sites as well as the subsequent catalytic reaction process. Therefore, the adsorption behavior of mercaptan molecules on La-Z5-F was investigated by CH_3SH-TPD and C_2H_5SH-TPD, as shown in Fig. 7. In RSH-TPD, the desorption temperature of CH_3SH (150–200 °C) is significantly higher than that of C_2H_5SH (80–150 °C), and the corresponding desorption area is significantly lower than that of C_2H_5SH, indicating that CH_3SH has a stronger binding ability with active sites that lead to a hard desorption, which might be one of reasons that the addition of CH_3SH seriously affects the catalytic decomposition of C_2H_5SH. Furthermore, it is found that there has a significant difference in the desorption products between CH_3SH and C_2H_5SH. As seen in Fig. 7A and 7B, two kinds of desorption of C_2H_4 and H_2S are detected for C_2H_5SH-TPD, while in addition to CH_4 and H_2S, the additional desorption products of CO_2 and CH_3SCH_3 are detected for CH_3SH-TPD. The difference in the desorption products indicates that the adsorption sites as well as the catalytic reaction and deactivation mechanism for decomposing CH_3SH and C_2H_5SH are different. Based on this result, the possible other deactivation causes are further invesitigated. First, the presence of CO_2 suggests the active oxygen species in La oxides over La/Z5-F as one of reaction sites participates in breaking C-S bond for decomposing CH_3SH. When C-S bond is broken, these active oxygen sites might also be attached by the nucleophilicity of sulfur that possibly deactivates the catalyst to some degree. Second, the appearance of CH_3SCH_3 is considered as the intermediate in decomposing CH_3SH ($CH_3SH \rightarrow CH_3SCH_3 \rightarrow CH_4 + H_2S$), which is deemed as another reaction pathway but also deactivates the catalyst. As known, CH_3SCH_3 is composed of one sulfur atom bonding with two methyl with a typical bent molecular configuration. This specific configuration results in the easier breakage of C-S bond so as to produce some deposited coke and sulfur, which is considered as one main reason for the quick catalyst deactivation. A comparison of an individual catalytic activity and stability experiments for decomposing single component of CH_3SCH_3, CH_3SH, C_2H_5SH and C_3H_7SH, respectively, over La-Z5-F was conducted to verify the above result, as shown in Fig. 7C and 7D. It is generally found that the shorter the carbon chain of mercaptan molecules, the worst the catalytic activity and the catalytic stability. Interestingly, CH_3SCH_3 molecule has the unique catalytic behavior, and exhibits the worst catalytic activity and stability. For example, when the temperature is below 350 °C, the conversion of CH_3SCH_3 is lower than 10%, while the temperature exceeds 375 °C, the conversion of CH_3SCH_3 is rapidly increased to 100%, indicating that the catalytic decomposition of CH_3SCH_3 is temperature-sensitive reaction and is different with those of other mercaptans. Moreover, the lifetime for decomposing CH_3SCH_3 is largely lower than those of other mercaptans, proving the low stability of CH_3SCH_3 molecule at high temperature. This reaction was confirmed to follow the equation of $CH_3SCH_3 = CH_4 + H_2S + C^*$ or CH_3SCH_3

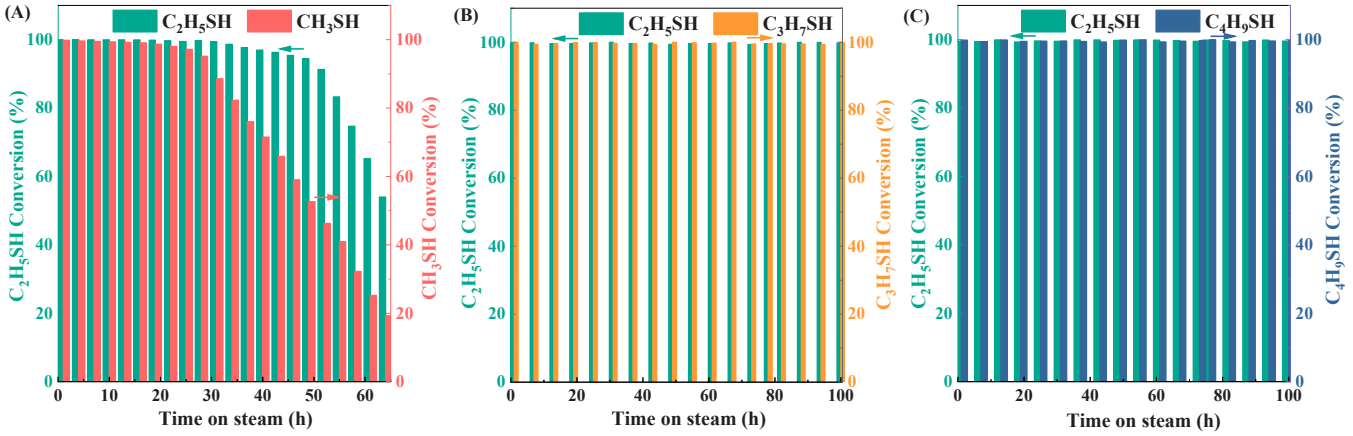

Fig. 6. Low-carbon mercaptans conversions in co-existed system as a function of time over La-Z5-F at 450 °C (A: C_2H_5SH/CH_3SH, B: C_2H_5SH/C_3H_7SH and C: C_2H_5SH/C_4H_9SH). Reaction conditions: m= 0.2 g, total sulfur concentration of 5000 ppm (all the concentration of CH_3SH, C_2H_5SH, C_3H_7SH, C_4H_9SH is equal to 2500 ppm), WHSV= 9 000 mL/(g·h).

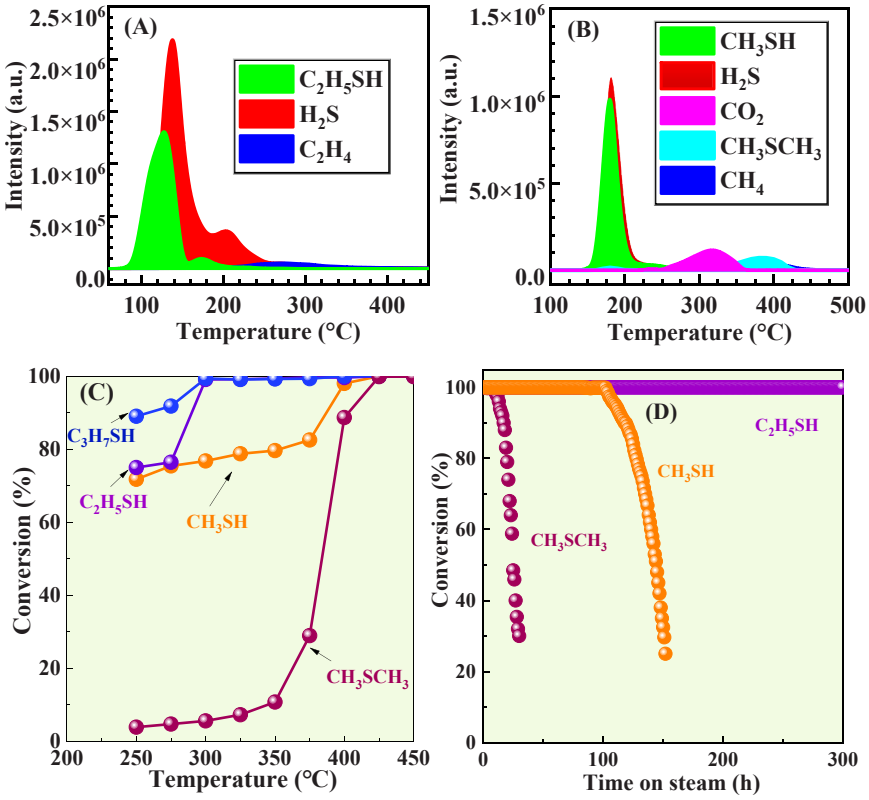

Fig. 7. (A) CH_3SH-TPD, (B) C_2H_5SH-TPD of La-Z5-F and (C) Conversion and (D) stability of single component of CH_3SCH_3, CH_3SH, C_2H_5SH, and C_3H_7SH over La-Z5-F sample (5000 ppm, 0.2 g, WHSV=9 000 mL/(g·h)).

$= CH_4 + H_2 + S^* + C^*$, as proved by CH_3SH-TPD in Fig. 7B and other reported literature [23,52,53]. In a word, it is speculated that all the hard desorption of CH_3SH, the poisoning of active oxygen by gaseous sulfur species as well as the deposition of solid coke and sulfur caused by the key intermediate of CH_3SCH_3 might be responsible for the rapid deactivation of La/Z catalysts in decomposing mixed CH_3SH and C_2H_5SH.

3.5. Exploring the effect of moisture

The prevalence of moisture impurity in industrial waste gases usually affects the performance of catalysts. Thus, the effect of moisture on the catalytic stability for decomposing a mixture of CH_3SH and C_2H_5SH over La-Z5-F catalyst was investigated. In order to simulate a more practical environment, a lower concentration of mixed mercaptans (reducing from 5000 ppm to 500 ppm), a higher WHSV (increasing from 9 000 mL/(g·h) to 15 000 mL/(g·h)), and the presence of moisture with a volume fraction of 10% were selected to investigate the water-resistance stability through a continuous cycles, as shown in Fig. 8. In the first 3 cycles (75 h), the addition of 10% moisture has no effect on their conversion for the degradation of mixed CH_3SH and C_2H_5SH, which shows a significant advantage compared to most of the available materials currently [54–56]. When the number of cycles is continued to increase (75–180 h), it is found that C_2H_5SH in mixed mercaptans is always completely converted in the presence of moisture, but the conversion for the degradation of CH_3SH drops to about 90% with a loss of 10%, which

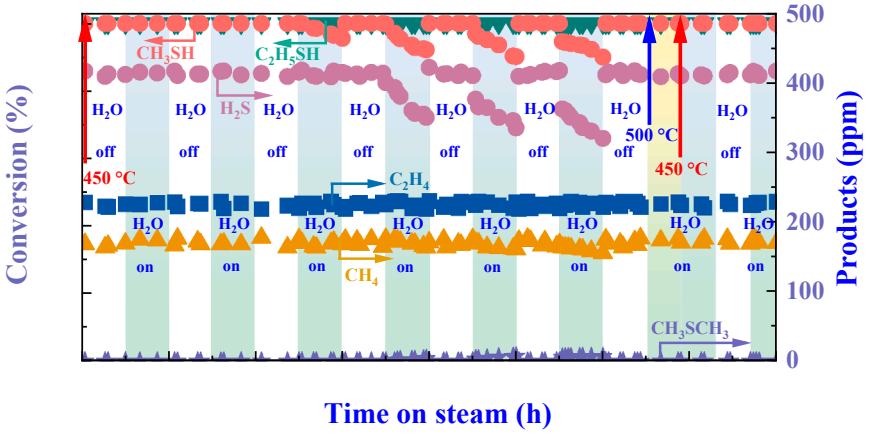

Fig. 8. Effects of moisture on CH_3SH and C_2H_5SH conversions as well as the corresponding products distribution over La-Z5-F catalyst. Reaction conditions: CH_3SH = 500 ppm, C_2H_5SH = 500 ppm, H_2O = 10%(v/v), WHSV= 15000 mL/(g·h) balanced with N_2 (the white area and violet area represent the experiments of H_2O-off and H_2O-on at 450 °C, respectively, and the orange area represents the reaction of H_2O-off at 500 °C).

clearly indicates that the active sites for the degradation of C_2H_5SH and CH_3SH are completely distinguished. It is well accepted that Brønsted acid is the main active site over ZSM-5 type zeolite, and lattice oxygen species can be acted as one of active site after the addition of La as confirmed by the generated CO_2 during the decomposition of CH_3SH. It is speculated that during the system of mixed mercaptans in the presence of moisture, the catalytic decomposition of C_2H_5SH mainly occurs over Brønsted acid site, and the catalytic decomposition of CH_3SH is inclined to occur preferentially on active oxygen site, followed by Brønsted acid site. Interestingly, once the moisture was switched off during the experiment, the conversion for the degradation of CH_3SH could still be restored to almost 100%. These results suggest that moisture possibly covers the active oxygen sites via weak hydrogen bonding interaction with a completed adsorption of CH_3SH, which induces the reversible deactivation [57–59]. To further investigate the role of moisture, the reaction temperature was increased from 450° to 500°C, and the sample was treated with moisture for another 10 h, and then the reaction temperature was reduced to 450 °C. It is found that the conversion of CH_3SH could be restored to almost 100% during the above circle and the following water-resistance circles. These results also confirm that the decrease in the CH_3SH conversion for decomposing mixed C_2H_5SH and CH_3SH with the presence of moisture over La-Z catalyst is possibly originated from the role of reversible water-induced deactivation. To reveal why water induces a reversible deactivation, La-Z5-F after stability test named as La-Z-R240 was further characterized by XRD, XPS, FT-IR, and TG to verify the surface microstructure and composition changes during water-resistant on-off experiment.

The XRD profiles of La-Z5-F and La-Z5-R240 are shown in Fig. S4, and the corresponding XPS, FT-IR and TG profiles are displayed in Fig. 9 A-F. It is shown in Fig. S4 that the crystalline phase structure of La-Z5-R240 catalyst is almost unchanged compared with that of fresh La-Z5-F, indicating that the phase structure is stable after the addition of moisture. XPS analysis was used to determine the amount and composition of carbon, oxygen and La species before and after the stability test. It is clear in Fig. 9A that La/Z-R240 does not detect any distinct sulfur species, including S^0 and SO_4^{2-} species [32], suggesting that moisture effectively suppresses the deposition of sulfur species during the reaction. The XPS spectra shows the presence of distinguished peaks corresponding to C 1 s and O 1 s, as shown in Figs. 9B and 9C, respectively. The binding energy of 284.8 eV is attributed to carbon atoms in the C-C/C-H fraction, and 286.2 eV and 288.6 eV are assigned to C-O and O-C═O in the carbonates or/and bicarbonates [60,61]. In water resistance experiments, the relative carbon content of C-C/C-H fraction decreases sharply from 84.2% to 47.97%, and the relative carbon content of the carbonates/bicarbonates increases from 15.8% to 52.03%, indicating that the reaction of deposited coke with moisture to produce a large number of carbonates that deposited on the catalyst surface or/and the reaction of CO_2 product with water to form bicarbonates. Similarly, the O 1 s XPS spectra confirms the formation of carbonates/bicarbonates. The binding energy of 530.9, 532.0, and 535.6 eV are assigned to oxygen in the La oxide, Si-O-Al, and O-C═O fractions, respectively [61]. The higher binding energy of O-C═O fractions suggests the formation of weak-interacted bicarbonates. An additional change is found that the decrease in the oxygen species of La oxide is followed by the increase in the oxygen content of the O-C═O fraction, which indicates that the reaction of CH_3SH with active oxygen of La oxides promotes the formation of CO_2, which is further reacted with water to generate a small amount of bicarbonates. Furthermore, as seen from the La 3d spectrum (Fig. 9D), the amount of La species in the catalyst decreased significantly after the reaction, probably because the increased (bi)carbonates deposition during the reaction. To further obtain the details on the type of coke composition, FT-IR analysis was carried out (Fig. 9E). As reported in literature, the vibrations of 1220 cm^{-1} and 1095 cm^{-1} are respectively associated with external connections between tetrahedra [62,63] and internal five-membered ring O-T-O asymmetric vibrations associated with AlO_4 tetrahedra [64]. A big difference is originated from the region of 1350–1700 cm^{-1}. It is found that a large peak at 1630 cm^{-1} proves the generation of a complex mixture of unsaturated hydrocarbons, i.e. the C═C stretching vibrations of polyolefins [65], which is probably derived from the deposition of ethene product during the decomposition of C_2H_5SH. More importantly, some obvious peaks at 1460 cm^{-1} as well as 1532 and 1400 cm^{-1} proves the formation of

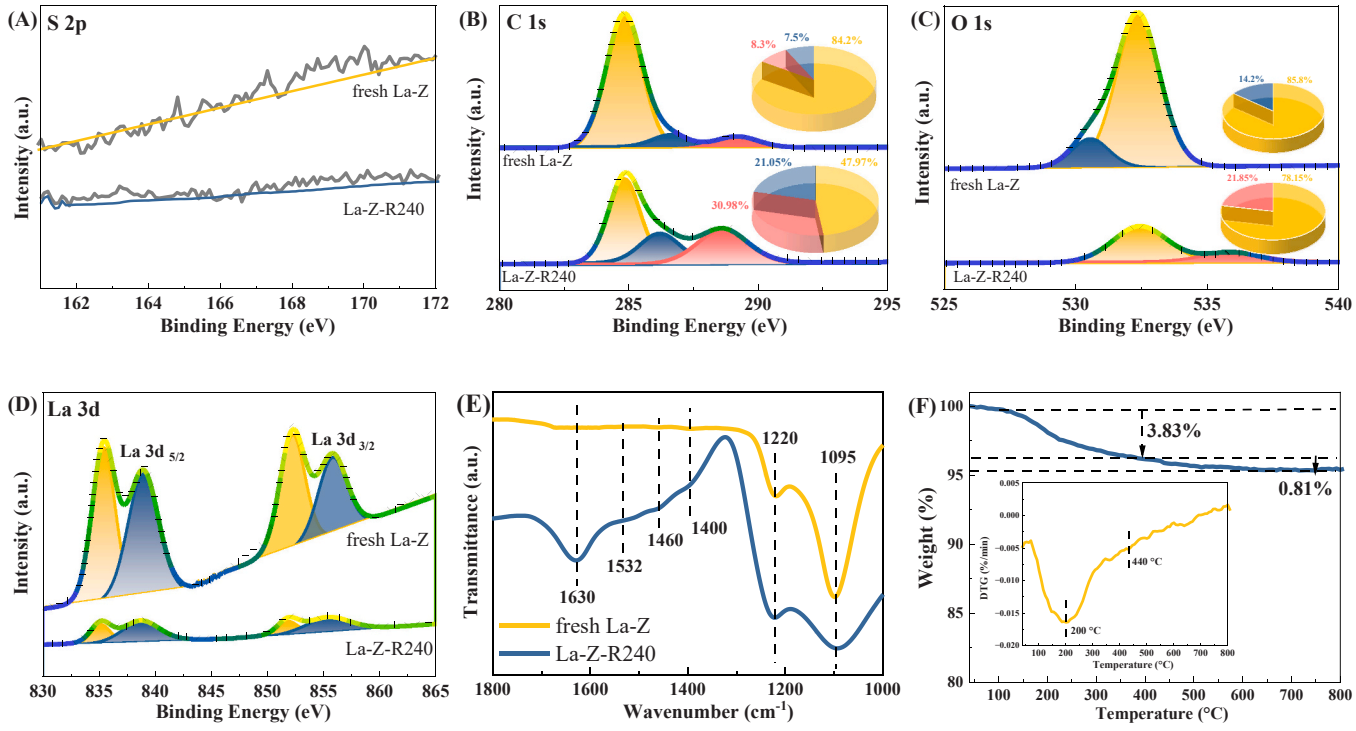

Fig. 9. (A) S 2p XPS spectra of fresh La-Z, and La-Z-R240 after stability. (B) C 1 s XPS spectra, (C) O 1 s XPS spectra, (D) La 3d XPS spectra, (E) FT-IR spectra of fresh La-Z and La-Z-R240, as well as (F) TG curves of La-Z-R240.

unsaturated and branched aliphatic hydrocarbons [66,67] and (bi)carbonate-like species [68,69], respectively. TG technique was used to verify the presence of the (bi)carbonate-like species and the TG result of La-Z-R240 is shown in Fig. 10F. In the first stage, the weight loss of 3.83% in the temperature range of 100–300 °C proves the presence of strongly adsorbed water molecules. In the second stage, the weight loss of 0.81% in the temperature range of 400–600 °C demonstrates the formation of surface carbonate and bicarbonate related species [70,71]. All the above results demonstrate that the inhibited role of water on the catalytic stability is to react with produced CO_2 as well as deposited carbon to form carbonate and bicarbonate related species that are accumulated over reactive oxygen sites leading to the reversible water-induced deactivation.

In summary, for the two components mixed system, methyl mercaptan had a strong negative influence on the stability for decomposing ethyl mercaptan, but propyl mercaptan and butyl mercaptan had essentially no influence on the stability of ethyl mercaptan. La-Z5-F catalyst showed good catalytic performance in the water resistance experiments. It was also demonstrated that the active site for the decomposition of ethyl mercaptan is mainly the acid site, whereas the active site for the decomposition of methyl mercaptan includes the acid site and the oxygen site (Fig. 10). Among them, the oxygen site is a dominant competitive site for decomposing CH_3SH. The addition of moisture only affects the decomposition of methyl mercaptan, but has no influence on decomposing ethyl mercaptan. During the reaction, it was demonstrated that the production of sulfur species is largely inhibited by a moisture atmosphere, and the produced CO_2 promotes the formation of carbonate-like species with the presence of moisture leading to a decrease in the stability for decomposing methyl mercaptan during the mixed system. However, a simple treatment by lifting the reaction temperature allowed the catalyst to return to its previous catalytic performance, which is beneficial for practical industrial applications.

4. Conclusions

In this work, the introduction of rare earths into ZSM-5 zeolite significantly enhanced the catalytic activity and stability for degradation of ethyl mercaptan. The reaction pathway and the causes of catalyst deactivation were revealed by a series of characterizations of XRD, N_2 adsorption and desorption, CO_2/NH_3-TPD, XPS, in situ DRIFTS, FT-IR, TG, and RSH-TPD, etc. The enhanced stability of La doped ZSM-5 catalyst was related to the changes in acidity and alkalinity that inhibited the deposition of coke and sulfur species and prevented the deactivation of the catalyst. In addition, the stability experiment for the catalytic degradation of mixed mercaptans was investigated. The effect of propyl mercaptan and butyl mercaptan on the catalytic decomposition of ethyl mercaptan was not obvious, while the effect of methyl mercaptan on catalytic decomposition of ethyl mercaptan was significant due to the presence of competing adsorption, the gaseous sulfur poisoning and the deposition of solid sulfur and coke. Moreover, a high moisture-resistance stability for decomposing mixed mercaptans with the presence of moisture was obtained, and the slight decrease in the CH_3SH conversion was originated from the competitive adsorption of moisture and the following moisture-induced deactivation, leading to the formation of carbonate and bicarbonate related species.

CRediT authorship contribution statement

Jichang Lu: Conceptualization, Methodology, Software, Investigation, Formal analysis, Writing – original draft. **Rui Tian:** Methodology, Investigation, Data curation, Writing – original draft. **Wenjun Zhang:** Visualization, Investigation; **Yilin Zhang:** Visualization. **Yijia Yang:** Software, Validation. **Zhizhi Xu:** Visualization, Writing – review & editing. **Dedong He:** Visualization, Investigation. **Tianhao Ai:** Conceptualization, Resources, Writing – review & editing. **Yongming Luo:** Conceptualization, Funding acquisition, Resources, Supervision, Writing – review & editing.

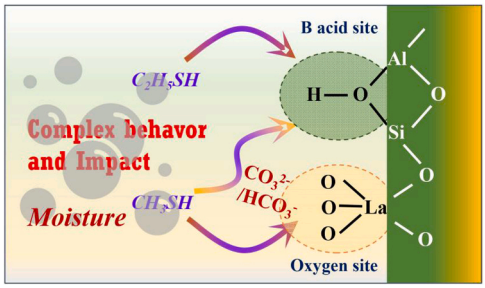

Fig. 10. The microstructure diagram for decomposing two components methyl and ethyl mercaptan under the presence of moisture on La-Z5-F catalyst.

Declaration of Competing Interest

The authors declare that they have no known competing financial interests or person relationships that could have appeared to influence the work reported in this paper.

Data availability

No data was used for the research described in the article.

Acknowledgments

The authors are grateful for the financial support from National Natural Science Foundation of China (Grant No. 42030712, 22106055 and 21966018), Major Science and Technology Projects in Yunnan Province (Grant No. 202302AG050002/KKAU202322028), Yunnan Applied Basic Research Projects (Grant No. 202301AW070019, 202101AS070026, 202201AT070086, 202101AU070025, 202101BE070001-026 and 202105AE160019) and Yunnan Province Xingdian Talent Support Project, KKRD202222054.

Appendix A. Supporting information

Supplementary data associated with this article can be found in the online version at doi:10.1016/j.apcatb.2023.123114.

References

[1] C. He, J. Cheng, X. Zhang, M. Douthwaite, S. Pattisson, Z. Hao, Recent advances in the catalytic oxidation of volatile organic compounds: a review based on pollutant sorts and sources, Chem. Rev. 119 (7) (2019) 4471–4568.
[2] C. Guo, J. Zhu, J. He, L. Hu, P. Zhang, D. Li, Catalytic oxidation/photocatalytic degradation of ethyl mercaptan on alpha-MnO_2@$H_4Nb_6O_{17}$-NS nanocomposite, Vacuum 182 (2020), 109718.
[3] Y. Lyu, X. Liu, W. Liu, Y. Tian, Z. Qin, Adsorption/oxidation of ethyl mercaptan on Fe-N-modified active carbon catalyst, Chem. Eng. J. 393 (2020), 124680.
[4] X. Zhang, L. Wang, L. Hu, J. He, Adsorption and separation of ethyl mercaptan from methane gas on HNb_3O_8 nanosheets, Ind. Eng. Chem. Res. 60 (2021) 8504–8515.
[5] J. Zhu, L. Hu, J. He, X. Zhang, C. Guo, Morphology and surface hydroxyl engineering of $H_4Nb_6O_{17}$ nanotubes for enhanced ethyl mercaptan removal, J. Nat. Gas. Sci. Eng. 94 (2021), 104133.
[6] C. Cammarano, E. Huguet, R. Cadours, C. Leroi, B. Coq, V. Hulea, Selective transformation of methyl and ethyl mercaptans mixture to hydrocarbons and H_2S on solid acid catalysts, Appl. Catal. B-Environ. 156 (2014) 128–133.
[7] M. Ziolek, P. Decyk, Relation between chemisorption and catalytic transformation of R_2S compounds on faujasite-type zeolites, Langmuir 15 (1999) 5781–5784.
[8] A.K. Vasiliou, D.E. Anderson, T.W. Cowell, J. Kong, W.F. Melhado, M.D. Phillips, J. C. Whitman, Thermal decomposition mechanism for ethanethiol, J. Phys. Chem. A 121 (2017) 4953–4960.
[9] V. Hosseinpour, M. Kazemeini, A. Mohammadi, A. Rashidi, Design, manufacture and application of a microreactor for the decomposition of ethyl mercaptan on an H-ZSM-5 catalyst, J. Clean. Prod. 292 (2021), 126036.
[10] J. Li, L. Xu, J. He, P. Zhou, L. Hu, D. Li, B. Wang, The structure feature of novel Cu_2O/e-HTi_2NbO_7 nanocomposite and their enhanced photocatalytic activity, Nano: Brief. Rep. Rev. 12 (2017) 1750100.

[11] J. He, L. Hu, Y. Tang, H. Li, P. Yang, Z. Li, Adsorption features and photocatalytic oxidation performance of $M_{1/3}NbMoO_6$ (M = Fe, Ce) for ethyl mercaptan, RSC Adv. 4 (2014) 22334–22341.
[12] H.E. Jie, Z. Jun-bin, L.A.N. Yun-xiang, Adsorption and photocatalytic oxidation of dimethyl sulfide and ethyl mercaptan over layered $K_{1-2x}Mn_xTiNbO_5$ and $K_{1-2x}Ni_xTiNbO_5$, J. Fuel Chem. Technol. 37 (2009) 485–488.
[13] M. Sedighi, F. Vahabzadeh, S.M. Zamir, A. Naderifar, Ethanethiol degradation by Ralstonia eutropha, Biotechnol. Bioprocess Eng. 18 (2013) 827–833.
[14] Q. Xiao, S. Cai, J. Liu, Microbial and thermogenic hydrogen sulfide in the Qianjiang Depression of Jianghan Basin: insights from sulfur isotope and volatile organic sulfur compounds measurements, Appl. Geochem. 126 (2021), 104865.
[15] Z. Sarbak, Desulfurization of ethanethiol over cadmium and mercury modified zeolite NaX, Appl. Catal. A-Gen. 147 (1996) 47–54.
[16] E. Huguet, B. Coq, R. Durand, C. Leroi, R. Cadours, V. Hulea, A highly efficient process for transforming methyl mercaptan into hydrocarbons and H_2S on solid acid catalysts, Appl. Catal. B-Environ. 134 (2013) 344–348.
[17] V. O'Shea, M.C. Alvarez-Galvan, J.L.G. Fierro, P.L. Arias, Influence of feed composition on the activity of Mn and $PdMn/Al_2O_3$ catalysts for combustion of formaldehyde/methanol, Appl. Catal. B-Environ. 57 (2005) 191–199.
[18] S.C. Kim, W.G. Shim, Catalytic combustion of VOCs over a series of manganese oxide catalysts, Appl. Catal. B-Environ. 98 (2010) 180–185.
[19] N. Burgos, M. Paulis, M.M. Antxustegi, M. Montes, Deep oxidation of VOC mixtures with platinum supported on Al_2O_3/Al monoliths, Appl. Catal. B-Environ. 38 (2002) 251–258.
[20] P.O. Larsson, A. Andersson, Oxides of copper, ceria promoted copper, manganese and copper manganese on Al_2O_3 for the combustion of CO, ethyl acetate and ethanol, Appl. Catal. B-Environ. 24 (2000) 175–192.
[21] J.I. Gutierrez-Ortiz, B. de Rivas, R. Lopez-Fonseca, J.R. Gonzalez-Velasco, Catalytic purification of waste gases containing VOC mixtures with Ce/Zr solid solutions, Appl. Catal. B-Environ. 65 (2006) 191–200.
[22] C. He, P. Li, J. Cheng, Z.P. Hao, Z.P. Xu, A. Comprehensive, Study of deep catalytic oxidation of Benzene, Toluene, ethyl acetate, and their mixtures over Pd/ZSM-5 catalyst: mutual effects and kinetics, Water Air Soil Pollut. 209 (2010) 365–376.
[23] R. Tian, J. Lu, Z. Xu, W. Zhang, J. Liu, L. Wang, Y. Xie, Y. Zhao, X. Cao, Y. Luo, Unraveling the synergistic reaction and the deactivation mechanism for the catalytic degradation of double components of sulfur-containing VOCs over ZSM-5-based materials, Environ. Sci. Technol. 57 (2023) 1443–1455.
[24] F. Bertinchamps, A. Attianese, M.M. Mestdagh, E.M. Gaigneaux, Catalysts for chlorinated VOCs abatement: multiple effects of water on the activity of VO_x based catalysts for the combustion of chlorobenzene, Catal. Today 112 (2006) 165–168.
[25] H. Pan, M. Xu, Z. Li, S. Huang, C. He, Catalytic combustion of styrene over copper based catalyst: Inhibitory effect of water vapor, Chemosphere 76 (2009) 721–726.
[26] P. Gelin, L. Urfels, M. Primet, E. Tena, Complete oxidation of methane at low temperature over Pt and Pd catalysts for the abatement of lean-burn natural gas fuelled vehicles emissions: influence of water and sulphur containing compounds, Catal. Today 83 (2003) 45–57.
[27] C.H. Wang, Al_2O_3-supported transition-metal oxide catalysts for catalytic incineration of toluene, Chemosphere 55 (2004) 11–17.
[28] H. Einaga, S. Futamura, Effect of water vapor on catalytic oxidation of benzene with ozone on alumina-supported manganese oxides, J. Catal. 243 (2006) 446–450.
[29] D. He, J. Yu, Y. Mei, J. Liu, Y. Zhao, S. Yang, X. Cao, S. He, Y. Luo, The effects of Cr addition in HZSM-5 on its structure, physicochemical and catalytic properties for methyl mercaptan abatement, Catal. Commun. 112 (2018) 31–34.
[30] D. He, D. Chen, H. Hao, J. Yu, J. Liu, J. Lu, G. Wan, S. He, K. Li, Y. Luo, Enhanced activity and stability of Sm-doped HZSM-5 zeolite catalysts for catalytic methyl mercaptan (CH_3SH) decomposition, Chem. Eng. J. 317 (2017) 60–69.
[31] D. He, Y. Zhao, S. Yang, Y. Mei, J. Yu, J. Liu, D. Chen, S. He, Y. Luo, Enhancement of catalytic performance and resistance to carbonaceous deposit of lanthanum (La) doped HZSM-5 catalysts for decomposition of methyl mercaptan, Chem. Eng. J. 336 (2018) 579–586.
[32] J. Lu, H. Hao, L. Zhang, Z. Xu, L. Zhong, Y. Zhao, D. He, J. Liu, D. Chen, H. Pu, S. He, Y. Luo, The investigation of the role of basic lanthanum (La) species on the improvement of catalytic activity and stability of HZSM-5 material for eliminating methanethiol-(CH_3SH), Appl. Catal. B-Environ. 237 (2018) 185–197.
[33] J. Liu, D. He, D. Chen, H. Hao, J. Yu, J. Lu, F. Liu, P. Liu, Y. Zhao, Y. Luo, Promotional effects of rare-earth (La, Ce and Pr) modification over HZSM-5 for methyl mercaptan catalytic decomposition, J. Taiwan Inst. Chem. Eng. 80 (2017) 262–268.
[34] J.A. Schellman, Thermodynamics, molecules and the Gibbs conference, Biophys. Chem. 64 (1997) 7–13.
[35] F. Macdonald, D.R. Lide, CRC handbook of chemistry and physics: from paper to web, Abstr. Pap. Am. Chem. Soc. 225 (2003). U552-U552.
[36] H.S. Peng, J. Tang, L. Yang, J.B. Pang, H.S. Ashbaugh, C.J. Brinker, Z.Z. Yang, Y. F. Lu, Responsive periodic mesoporous polydiacetylene/silica nanocomposites, J. Am. Chem. Soc. 128 (2006) 5304–5305.
[37] J. Bi, M. Liu, C. Song, X. Wang, X. Guo, C-2-C-4 light olefins from bioethanol catalyzed by Ce-modified nanocrystalline HZSM-5 zeolite catalysts, Appl. Catal. B-Environ. 107 (2011) 68–76.
[38] D. He, H. Hao, D. Chen, J. Liu, J. Yu, J. Lu, F. Liu, S. He, K. Li, Y. Luo, Effects of rare-earth (Nd, Er and Y) doping on catalytic performance of HZSM-5 zeolite catalysts for methyl mercaptan (CH_3SH) decomposition, Appl. Catal. A-Gen. 533 (2017) 66–74.
[39] J. Ouyang, F. Kong, G. Su, Y. Hu, Q. Song, Catalytic conversion of bio-ethanol to ethylene over La-Modified HZSM-5 catalysts in a bioreactor, Catal. Lett. 132 (2009) 64–74.
[40] W. Monama, E. Mohiuddin, B. Thangaraj, M.M. Mdleleni, D. Key, Oligomerization of lower olefins to fuel range hydrocarbons over texturally enhanced ZSM-5 catalyst, Catal. Today 342 (2020) 167–177.
[41] L. Peng, Z. Wei, C. Wan, J. Li, Z. Chen, D. Zhu, D. Baumann, H. Liu, C.S. Allen, X. Xu, A.I. Kirkland, I. Shakir, Z. Almutairi, S. Tolbert, B. Dunn, Y. Huang, P. Sautet, X. Duan, A fundamental look at electrocatalytic sulfur reduction reaction, Nat. Catal. 3 (2020) 762–770.
[42] X. Yue, S. Wang, D. Li, Y. Zhao, S. Wang, W. Ding, Experimental and numerical investigations on the adsorption/desorption performance of low-concentration VOCs over H-ZSM-5 with different SiO_2/Al_2O_3 ratios, Ind. Eng. Chem. Res. 62 (2023) 5408–5419.
[43] H. Huang, W. Rong, Y. Gu, R. Chang, H. Lu, Adsorption and desorption of VOCs on the ZSM-5 zeolite, Acta Sci. Circumstantiae 34 (2014) 3144–3151.
[44] J. Zhang, W. Yin, H. Shang, C. Liu, In situ FT-IR spectroscopy investigations of carbon nanotubes supported Co-Mo catalysts for selective hydrodesulfurization of FCC gasoline, J. Nat. Gas. Chem. 17 (2008) 165–170.
[45] S. Bai, Y. Xu, P. Wang, Q. Shao, X. Huan, Activating and converting CH_4 to CH_3OH via the $CuPdO_2$/CuO nanointerface, ACS Catal. 9 (2019) 6938–6944.
[46] J. Miao, L. Yuan, Q. Guan, G. Liang, A. Gu, Water-phase synthesis of a biobased Allyl compound for building UV-Curable flexible thiol ene polymer networks with high mechanical strength and transparency, ACS Sustain. Chem. Eng. 6 (2018) 7902–7909.
[47] W. Zhao, B. Song, J. Tao, J. Zhang, M. Huang, C. Wang, M. Gou, Thiol-functionalized mesoporous silica for effective trap of mercury in rats, J. Nanomater. 2016 (2016) 9758264.
[48] A. Lazauskas, D. Jucius, V. Baltrusaitis, R. Gudaitis, I. Prosycevas, B. Abakeviciene, A. Guobiene, M. Andrulevicius, V. Grigaliunas, Shape-memory assisted scratch-healing of transparent thiol-ene coatings, Materials 12 (2019) 482.
[49] J. Luis Sotelo, G. Ovejero, A. Rodriguez, S. Alvarez, J. Galan, J. Garcia, Competitive adsorption studies of caffeine and diclofenac aqueous solutions by activated carbon, Chem. Eng. J. 240 (2014) 443–453.
[50] Z. Li, L. Sellaoui, G.L. Dotto, A. Bonilla-Petriciolet, A. Ben, Lamine, Understanding the adsorption mechanism of phenol and 2-nitrophenol on a biopolymer-based biochar in single and binary systems via advanced modeling analysis, Chem. Eng. J. 371 (2019) 1–6.
[51] Z. Li, L. Sellaoui, D. Franco, M.S. Netto, J. Georgin, G.L. Dotto, A. Bajahzar, H. Belmabrouk, A. Bonilla-Petriciolet, Q. Li, Adsorption of hazardous dyes on functionalized multiwalled carbon nanotubes in single and binary systems: Experimental study and physicochemical interpretation of the adsorption mechanism, Chem. Eng. J. 389 (2020), 124467.
[52] D. He, H. Hao, D. Chen, J. Lu, L. Zhong, R. Chen, F. Liu, G. Wan, S. He, Y. Luo, Rapid synthesis of nano-scale CeO_2 by microwave-assisted sol–gel method and its application for CH_3SH catalytic decomposition, J. Environ. Chem. Eng. 4 (2016) 311–318.
[53] X. Cao, J. Lu, X. Zheng, D. He, W. Zhu, Y. Zhao, W. Zhang, R. Tian, Y. Luo, Regulation of the reaction pathway to design the high sulfur/coke-tolerant Ce-based catalysts for decomposing sulfur-containing VOCs, Chem. Eng. J. 429 (2022) 1–13.
[54] N. Laosiripojana, S. Assabumrungrat, Conversion of poisonous methanethiol to hydrogen-rich gas by chemisorption/reforming over nano-scale CeO_2: The use of CeO_2 as catalyst coating material, Appl. Catal. B: Environ. 102 (2011) 267–275.
[55] W. Qu, Z. Tang, W. Liu, Y. Liao, Y. Huang, D. Xia, Q. Lian, S. Tian, C. He, D. Shu, Self-accelerating interfacial catalytic elimination of gaseous sulfur-containing volatile organic compounds as microbubbles in a facet-engineered three-dimensional BiOCl Sponge fenton-like process, Environ. Sci. Technol. 56 (2022) 11657–11669.
[56] D. Ma, W. Liu, Y. Huang, D. Xia, Q. Lian, C. He, Enhanced catalytic ozonation for eliminating CH3SH via stable and circular electronic metal–support interactions of Si–O–Mn bonds with low mn loading, Environ. Sci. Technol. 56 (2022) 3678–3688.
[57] Z. Shi, P. Yang, F. Tao, R. Zhou, New insight into the structure of CeO_2-TiO_2 mixed oxides and their excellent catalytic performances for 1,2-dichloroethane oxidation, Chem. Eng. J. 295 (2016) 99–108.
[58] Q. Dai, J. Wu, W. Deng, J. Hu, Q. Wu, L. Guo, W. Sun, W. Zhan, X. Wang, Comparative studies of P/CeO_2 and Ru/CeO_2 catalysts for catalytic combustion of dichloromethane: from effects of H_2O to distribution of chlorinated by-products, Appl. Catal. B-Environ. 249 (2019) 9–18.
[59] P. Yang, S. Yang, Z. Shi, F. Tao, X. Guo, R. Zhou, Accelerating effect of ZrO_2 doping on catalytic performance and thermal stability of CeO_2-CrO_x mixed oxide for 1,2-dichloroethane elimination, Chem. Eng. J. 285 (2016) 544–553.
[60] Z. Liu, L. Niu, X. Zong, L. An, D. Qu, X. Wang, Z. Sun, Ambient photothermal catalytic CO oxidation over a carbon-supported palladium catalyst, Appl. Catal. B-Environ. 313 (2022), 121439.
[61] B. Sivaranjini, R. Mangaiyarkarasi, V. Ganesh, S. Umadevi, Vertical alignment of liquid crystals over a functionalized flexible substrate, Sci. Rep. 8 (2018) 8891.
[62] S. Hamid, M.A. Kumar, W. Lee, Highly reactive and selective Sn-Pd bimetallic catalyst supported by nanocrystalline ZSM-5 for aqueous nitrate reduction, Appl. Catal. B-Environ. 187 (2016) 37–46.
[63] A. Cihanoglu, G. Gunduz, M. Dukkanci, Degradation of acetic acid by heterogeneous Fenton-like oxidation over iron-containing ZSM-5 zeolites, Appl. Catal. B-Environ. 165 (2015) 687–699.
[64] H.Y. Chen, L. Chen, J. Lin, K.L. Tan, J. Li, Copper sites in copper-exchanged ZSM-5 for CO activation and methanol synthesis: XPS and FTIR studies, Inorg. Chem. 36 (1997) 1417–1423.
[65] L. Lin, W. Lin, Y.X. Zhu, B.Y. Zhao, Y.C. Xie, G.Q. Jia, C. Li, Uniformly carbon-covered alumina and its surface characteristics, Langmuir 21 (2005) 5040–5046.

[66] M. Rozwadowski, M. Lezanska, J. Wloch, K. Erdmann, R. Golembiewski, J. Kornatowski, Investigation of coke deposits on Al-MCM-41, Chem. Mater. 13 (2001) 1609–1616.
[67] A.T. Aguayo, P. Castano, D. Mier, A.G. Gayubo, M. Olazar, J. Bilbao, Effect of Cofeeding Butane with Methanol on the Deactivation by Coke of a HZSM-5 Zeolite Catalyst, Ind. Eng. Chem. Res. 50 (2011) 9980–9988.
[68] X. Yi, Z. Xu, Y. Liu, X. Guo, M. Ou, X. Xu, Highly efficient removal of uranium(VI) from wastewater by polyacrylic acid hydrogels, RSC Adv. 7 (2017) 6278–6287.
[69] S.E. Noriega, A. Subramanian, Consequences of neutralization on the proliferation and cytoskeletal organization of chondrocytes on chitosan-based matrices, Int. J. Carbohydr. Chem. 2011 (2011), 809743.
[70] Z. Zhao, G. Li, Y. Sun, N. Li, Z. Zhang, J. Cheng, C. Ma, Z. Hao, The positive effect of water on acetaldehyde oxidation depended on the reaction temperature and MnO_2 structure, Appl. Catal. B-Environ. 303 (2022), 120886.
[71] Y. Zhang, Z. Wei, Y. Zhu, S. Tao, M. Chen, Z. Zhang, Z. Jiang, W. Shangguan, RE-NiO_x (RE=Ce, Y, La) composite oxides coupled plasma catalysis for benzene oxidation and by-product ozone removal, J. Rare Earths 41 (5) (2023) 789.